



HAL
open science

Characterization of photophysical and electrochemical properties of a PNDT-T-DPP dye-based polymer with highly planar features and development of organic electronic applications

Jinyang Chen, Yue Zhao, Wenxiang Zeng, Pingping Ni, Yujie Wang, Shuchang Chen, Xianhe Yuan, Zhuowen Feng, Suhong Tang, Sichun Wang, et al.

► To cite this version:

Jinyang Chen, Yue Zhao, Wenxiang Zeng, Pingping Ni, Yujie Wang, et al.. Characterization of photophysical and electrochemical properties of a PNDT-T-DPP dye-based polymer with highly planar features and development of organic electronic applications. *Dyes and Pigments*, 2025, 234, pp.112536. 10.1016/j.dyepig.2024.112536 . hal-04795204

HAL Id: hal-04795204

<https://hal.science/hal-04795204v1>

Submitted on 21 Nov 2024

HAL is a multi-disciplinary open access archive for the deposit and dissemination of scientific research documents, whether they are published or not. The documents may come from teaching and research institutions in France or abroad, or from public or private research centers.

L'archive ouverte pluridisciplinaire **HAL**, est destinée au dépôt et à la diffusion de documents scientifiques de niveau recherche, publiés ou non, émanant des établissements d'enseignement et de recherche français ou étrangers, des laboratoires publics ou privés.

Characterization of photophysical and electrochemical properties of a PNDT-T-DPP dye-based polymer with highly planar features and development of organic electronic applications

Jinyang Chen,¹ Yue Zhao,² Wenxiang Zeng,² PingPing Ni,³ Yujie Wang,⁴ Shuchang Chen,² Xianhe Yuan,² Zhuowen Feng,² Suhong Tang,² Sichun Wang,² Shiwei Ren,^{*2,5} and Abderrahim Yassar,^{*3}

¹ Alternative Technologies for Fine Chemicals Process of Zhejiang Key Laboratory, Shaoxing University, Shaoxing 312000, China

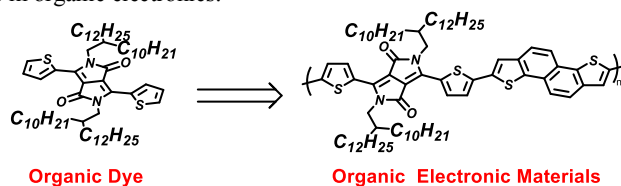
² National Key Laboratory for Processed Food Additives Assay, Gongbei Customs Technical Center, Gongbei Customs, Zhuhai 519001, China

³ LPICM-CNRS, Ecole Polytechnique, Institut Polytechnique de Paris, Palaiseau 91128, France

⁴ School of Luoyang Foreign Language, Luoyang 471000, China

⁵ Laboratory of Molecular Materials and Devices, Department of Materials Science, Fudan University, Shanghai 200438, China
shiwei_ren@fudan.edu.cn

Abstract. Common organic small molecule dyes exhibit chemical modifiability and are easy to polymerize, making them potential monomers in organic electronics. The multifunctionality of organic synthetic chemistry allows for material adaptability. Here, we report the synthesis route and purification methods for dye polymer based on thiophene-diketopyrrolopyrrole. Their orderly conjugated structure and high coplanarity contribute to a high crystallinity, which is favorable for charge carrier transport. By adjusting the device structure and thin film preparation conditions, the hole transport properties of the materials were further optimized, achieving a maximum mobility of up to $0.35 \text{ cm}^2 \text{ V}^{-1} \text{ s}^{-1}$. The excellent charge carrier performance reveals the potential of such materials for applications in organic electronics.



Highlight: Dye-based organic electronic material, highly coplanar structure, solution processing method, high mobility

1 Introduction

With a large delocalized π -electron system and excellent charge carrier mobility, π -conjugated molecules are fascinating materials for fabrication of solution-processed organic electronic devices

.¹⁻³ In comparison to inorganic materials, organic semiconductor materials are gaining attention due to their flexibility, light weight, easy functionalisation, variability, sustainability and low manufacturing costs.⁴⁻⁶ Typical organic optoelectronic applications refer to field effect transistors, electrochemical transistors, organic thermoelectric generators, solar cells, chemical sensors, etc., all of which use small organic molecules and/or polymers as the core components that modulate device performance.⁷⁻¹¹

Field effect transistors have been the focus of extensive research, especially solution processed polymers for transistor applications, known as polymer field effect transistors (PFETs).^{12, 13} This is due to the fact that solution processed polymer semiconducting materials have good film-forming capability and solution-processing properties compared to small-molecule semiconducting materials processed by thermal evaporation method.¹⁴ Common organic transistors are regularly classified into four construction types: top-gate top contacts, top-gate bottom contacts, bottom-gate top contacts and bottom-gate bottom contacts.¹⁵ Different construction structures can also have an impact on the performance of the device. A typical solution processed polymer skeleton consists of an alternating donor-acceptor (D-A) arrangement, which can be flexibly tuned to the frontier molecular orbital (FMO) energy level of the material by chemical structure design.¹⁶ The FMO energy levels include the highest occupied molecular orbital energy level (HOMO) and the lowest unoccupied molecular orbital energy level (LUMO), which are determined by the types and proportions of donors and acceptors in the materials, respectively.^{17, 18}

Exemplifying the acceptor group is the diketopyrrolopyrrole (DPP), which contains two lactam electron-withdrawing functional groups. On the other hand, DPP is an important class of synthetic dyes present in customs inspection, with outstanding properties such as bright colors, excellent photochemical and thermal stability.¹⁹⁻²² It has received a lot of attention due to its inclusion of thiophene groups and potentially halogen-containing atoms, which can lead to convenient polycondensation reactions for the preparation of polymers with long π -conjugations.^{23, 24} The donor unit tends to contain groups with strong electron-donating ability, while the acceptor unit often required to have a strong electron-withdrawing group. Naphtho[1,2-b:5,6-b']dithiophene (NDT) is a donor building block consisting of a naphthalene ring fused with two thiophene rings, forming thus a rigid, planar structure with an extended π -conjugated system. When incorporated into donor-acceptor copolymers, NDT units help create materials with tailor-made optoelectronic properties. This is due to their structural rigidity and high coplanarity, which reduce both the stacking distance between conjugated backbones and the polymers' reorganization energy, which enhance intermolecular interactions thereby resulting in high charge carrier mobility. Most of reported works mainly rely on the NDT carrying alkoxy or alkyl side chains. Takimiya et al. reported a series of copolymers incorporating NDT3 and its derivatives linked at the naphthalene positions in the copolymer backbone, and the copolymer exhibited a moderate hole mobility of

$10^{-2} \text{ cm}^2 \text{ V}^{-1} \text{ s}^{-1}$.²⁵ The same group has also developed a series of NDT with linear and angular shapes based polymers with alkyl-thiophene units and systematically investigated the relationship between organic transistor mobility and the NDT shape. The polymers bearing an angular-shaped NDT, exhibited the highest mobilities of $\sim 0.8 \text{ cm}^2 \text{ V}^{-1} \text{ s}^{-1}$.²⁶

It is rational to expect that incorporating unsubstituted NDT a larger polycyclic aromatic core into donor-acceptor copolymers would allow a short distance of π - π which would give rise to a more highly ordered microstructure, in turn yielding a high charge carrier mobility. Although many of NDT isomers and its derivatives have been synthesized and studied, however D-A copolymers containing unsubstituted NDT as donor units have not been synthesized to date, nor have their mesoscale supramolecular organization and charge carrier mobilities been investigated. In the present work, a novel D-A copolymer with NDT and DPP as donor and acceptor units respectively, as depicted in scheme 1, was synthesized, and its photophysical, microstructure organization and electrical properties were studied. The main design idea is to explore how unsubstituted NDT building block based material on an alternating linkage manner between two primitive blocks with high planar regularity, relying on C-C bonds while further improving the planarity of the material skeleton, impacts the effective intramolecular and intermolecular charge transport.

1.1 Experimental

Raw materials such as potassium carbonate (K_2CO_3), 9-(bromomethyl)nonadecane, *N*-bromosuccinimide (NBS) and organic solvents such as dimethylformamide (DMF), dichloromethane (DCM), petroleum ether (PE), ethyl acetate (EA) etc. were acquired from Guangzhou Chemical Reagent Factory (Guangzhou, China). Reaction precursor 3,6-di(thiophen-2-yl)-2,5-dihydropyrrolo[3,4-*c*]pyrrole-1,4-dione (T-DPP) and 2,7-bis(trimethylstannyl)naphtho[1,2-*b*:5,6-*b'*]dithiophene (NDT-SnMe₃) were purchased from SunaTech (China) and used directly. Catalyst tris(dibenzylideneacetone)dipalladium and ligand tri(*o*-tolyl)phosphine were purchased from Merck (Darmstadt, German) and stored for long periods of time in a nitrogen-filled glove box, referred to as $[\text{Pd}_2(\text{dba})_3]$ and $\text{P}(\text{o-ty})_3$, respectively. The preparation of intermediates and final dye polymer PNDT-T-DPP was described as follows.

1.2 Synthesis procedures for monomer T-DPP-Br

To a solution of T-DPP (2.10 g, 7.00 mmol, 1.00 equiv) in anhydrous DMF (25.0 mL) under an argon atmosphere protection, K_2CO_3 (2.42 g, 17.5 mmol, 2.50 equiv) was added in portions. Stirring was turned on and the mixture was warmed up to 80 °C to 85 °C and kept for half an hour. It was observed that almost all the solids were dissolved and the solution was red-brown in color. Subsequently, 11-(bromomethyl)tricosane (6.28 g, 15.05 mmol, 2.15 equiv) was injected dropwise into a three-necked flask through a syringe over a period of 10 minutes. The flow of argon was halted and the mixture was refluxed at 100 °C overnight. The mixture was brought to room temperature and the DMF solvent was removed by distillation under reduced pressure. The

organic phase was extracted three times by DCM, dried with sodium sulfate and filtered. After removal of the solvent under reduced pressure, the residue was purified by silica gel chromatography with the eluent being PE and DCM (4:1). The intermediate of 2,5-bis(2-octylododecyl)-3,6-di(thiophen-2-yl)-2,5-dihydropyrrolo[3,4-c]pyrrole-1,4-dione (5.13 g, 85.2 %) was obtained as the red powder and used directly. The foregoing red powder (2.00 g, 2.32 mmol, 1.00 equiv) from the previous step and NBS (0.85 g, 4.76 mmol, 2.05 equiv) were taken in a single-necked flask, followed by the addition of chloroform (6.0 mL). The mixture was heated to 65 °C under stirring conditions for 20 minutes. The reaction terminal was detected by thin layer chromatography and extracted promptly. After removal of the solvent under reduced pressure, the residue was purified by silica gel chromatography with the eluent being PE and DCM (5:2). T-DPP-Br (2.12 g, 89.8 %) was obtained as the red powder. ¹H NMR (400 MHz, Chloroform-d, ppm) δ 8.62 (d, J = 4.2 Hz, 2H), 7.21 (d, J = 4.2 Hz, 2H), 3.92 (d, J = 7.7 Hz, 4H), 1.93 – 1.82 (m, 2H), 1.25 (d, J = 27.9 Hz, 64H), 0.87 (q, J = 6.4 Hz, 12H). ¹³C NMR (100 MHz, Chloroform-d, ppm) 161.39, 139.39, 135.29, 131.42, 131.18, 118.94, 108.02, 46.35, 37.76, 31.92, 31.88, 31.18, 29.97, 29.63, 29.55, 29.49, 29.35, 29.28, 26.17, 22.69, 22.66, 14.11. NMR spectra were placed in Figures S1 and S2 in the Supplementary Information (SI). Mass: Calculated for [C₆₂H₁₀₃Br₂N₂O₂S₂]⁺: 1132.4454; Found: 1132.4458.

1.3 Synthesis procedure for dye polymer PNDT-T-DPP

The Schlenk tube (30 mL) was pre-dried sufficiently (150 °C) by oven and discharged with argon gas circulated three times to ensure an anhydrous and oxygen-free reaction environment. T-DPP-Br (225.7 mg, 0.20 mmol, 1.00 equiv), NDT-SnMe₃ (113.6 mg, 0.20 mmol, 1.00 equiv), [Pd₂(dba)₃] (5.49 mg, 6.0 μmol, 3 %) and P(o-ty)₃ (4.87 mg, 16.0 μmol, 8 %) were added sequentially and dissolved in dry chlorobenzene (9.0 mL). Argon gas was continued until the reaction temperature reached 130 °C. The gas was removed and the reaction was carried out under stirring. Argon was removed and the reaction was terminated after 72 hours under stirring conditions and the color of the polymerized system changed from pink to dark green with a viscous consistency. After slowly returning to room temperature, the mixture was pipetted dropwise into methanol solvent. The solid precipitate was filtered and transferred to a Soxhlet thimble and then Soxhlet extraction commenced.²⁷ Methanol, acetone, hexane and EA were used sequentially to remove unreacted monomers and short chain oligomers from the system under reflux conditions at 90 °C (12 h for each). The target product was dissolved in chloroform solution and was dark green in color. The solution containing the target product was added dropwise to methanol again and collected by filtration. The dye polymer PNDT-T-DPP was obtained by drying under reduced pressure (214.7 mg, 88.7 % yield). The ¹H NMR spectrum of the polymer shows broad peaks and was placed at Figure S3. The typical resonance peaks is qualitatively attributed to the respective fragments, including alkyl chains (0.5-2.0 ppm), amides (~ 5.5 ppm), and thiophenes in different subregions.

1.4 Characterization details of dye polymer PNDT-T-DPP

The molecular weight of dye polymer was assessed by gel permeation chromatography (eluent: trichlorobenzene, 140-150 °C, Agilent PL-GPC220, USA). The eluent was chosen to be trichlorobenzene to ensure sufficient solubility of the extended conjugated skeleton. Polystyrene-divinylbenzene and polystyrene were used as stationary phase and reference, respectively. The polymer solution at a concentration of 0.1 mg/mL was passed at a flow rate of 1.0 mL/min through a column (2* PLgel 10 µm MIXED-B). Thermal decomposition of powder (4.3 mg) was analyzed by thermogravimetry analysis (TGA, TA Discovery 550) in a nitrogen atmosphere (N₂). A differential scanning calorimeter (DSC, NETZSCH) was used to measure the temperature dependence of the physical properties of solid powders in N₂ atmosphere with a heating rate of 10 °C/minute, consisting of a first heating process (heating from room temperature to 250 °C), a first cooling process (cooling from 250 °C to room temperature) and a second heating process (heating from room temperature to 250 °C). Infrared and elemental analyses were performed on the powder (2.0 mg) and measured in both the Fourier transform infrared (FTIR) spectrometer and the organic elemental analyser (CHN mode of Elementar Vario), respectively. Photochemical characterization was performed on the ultraviolet-visible spectrometer (UV-2600, Shimadzu). Preparation in solution form: 0.5 mg of polymer powder was weighed and dissolved in 2 mL of chloroform solvent to obtain a greenish colored solution which was pipetted into a cuvette for testing. Preparation of thin film: The polymer solution prepared above was spin-coated onto a pre-cleaned quartz plate (1.0 x 2.0 cm²) and the solvent was then allowed to evaporate at 80 °C to prepare a thin film for testing. Electrochemical tests were carried out in acetonitrile solution containing tetrabutylammonium hexafluorophosphate. The three-electrode system in cyclic voltammetry (CV) is as follows: an Ag/AgCl (0.01 M) electrode, a glassy carbon electrode, and a platinum electrode are used as the reference, working, and counter electrodes, respectively. A drop of 10 µL of chloroform solution of the polymer was pipetted onto a 4 mm diameter glassy carbon electrode and subsequently allowed to evaporate slowly to form a dense film. The specific formula is as follows: $E_{\text{HOMO}} = -4.80 - (E_{\text{ox}}^{\text{onset}} - 0.40) \text{ eV}$, $E_{\text{LUMO}} = -4.80 - (E_{\text{red}}^{\text{onset}} - 0.40) \text{ eV}$. In which $E_{\text{ox}}^{\text{onset}} / E_{\text{red}}^{\text{onset}}$ was relative to the measured oxidation/reduction potential value of the Fc/Fc⁺ redox pair. Atomic force microscopy (AFM) measurements were performed on annealed samples in the thin film state (Dimension Icon, Burker, Germany). The grazing incidence wide angle X-ray scattering (GIWAXS) measurements were obtained at the 14 B/15 U beamline station from the Synchrotron Radiation Facility (Shanghai, China). The samples were tested using the same methodology as employed for PFET device performance analysis.

1.5 Device fabrication for measuring charge carrier mobility of dye polymer

Bottom gate top contact (BG/TC) PFETs were fabricated on a Si/SiO₂ substrate (1.5 cm × 1.5 cm). The substrates were ultrasonic by deionized water, ethanol, and isopropanol, then a piranha solution for 30 minutes, and then washed with deionized water and ethanol. p-Si substrate acted as a gate electrode, while SiO₂ was served as a gate dielectric. To further modify the interface, the SiO₂ surface was functionalized with

octadecyltrichlorosilane (OTS) using the self-assembled molecular layer method. The OTS modification can reduce the interfacial defects between the organic semiconductor layer and the dielectric layer and improve the flatness of the SiO₂ surface. The channel width and length of the field effect transistor devices used were 1400 μm and 30 μm, respectively. The dye polymer PNDT-T-DPP were pre-dissolved in chlorobenzene under thermal conditions and stirred overnight to fully dissolve (60 °C, 8.0 mg/mL). The solution was then deposited onto the substrate at a constant spin-coating rate of 3000 rpm under ambient conditions to form a thin film. Finally, the polymer film is annealed at 150 °C for a period of 30 minutes to eliminate the residual solvent to complete the fabrication of the device. Both source and drain electrodes were gold (Au, ~ 30 nm), (thermally deposited by evaporation. The transfer and output curves of PFFT were characterized using a 4200-semiconductor characterization system (Keithley, USA) operating in a nitrogen glove box. The construction of the device for Bottom gate bottom contact (BG/BC) is similar to that above, with only the order of preparation of the polymer film differing. The saturation hole mobility (μ) was calculated by the formula of:
$$\mu = \left(\frac{\partial \sqrt{|I_{DS}|}}{\partial V_{GS}}\right)^2 \cdot \frac{2L}{WC_i}$$
 (I_{DS} and V_{GS} refer to the source-drain current and gate voltage, respectively. L and W are the channel length and width, and their ratio is 5 ($W=280$, $L=1400$). C_i is the capacitance per unit area of the gate dielectric layer and is 11.5×10^{-9}).

1.6 Organic photodiodes device fabrication and characterization

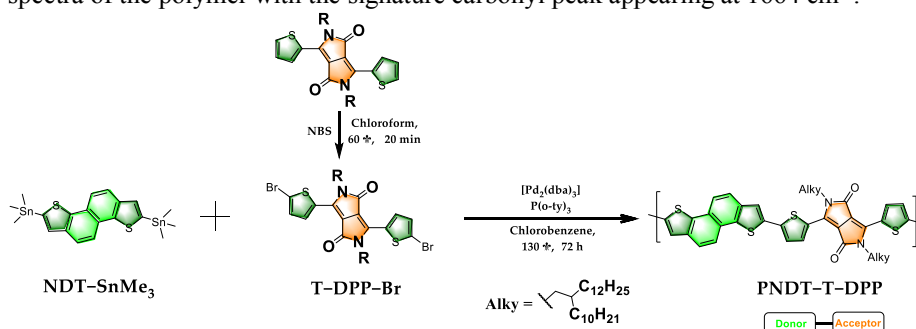
Firstly, ITO glasses with sheet resistance of 15 Ω cm⁻² and transmittance of 82% were cleaned with deionized water and ultrasonic treatment with the standard procedure (deionized water, ace-tone, and isopropanol for 15 minutes each). Subsequently, the cleaned ITO glass substrates were dried with nitrogen gas flow. Next, ITO glass substrates were treated with oxygen plasma (100 W, 10 minutes) to obtain a hydrophilic surface for subsequent spin-coating processes. PNDT-T-DPP (14 mg) and PCBM (14 mg) were dissolved in 1 mL chloroform solvent, filtered mixed solution was spin-coated onto the ITO glass substrate at a rotation speed of 2000 rpm and annealed at 80 °C for 5 minutes. Then, the substrates were transferred into the evaporation system to conduct the Al deposition processes. The device was characterized at room temperature under ambient laboratory conditions.

2 Results and discussion

Synthesis routes to polymer PNDT-T-DPP through Stille coupling polymerization

The polymerization was accomplished by means of a palladium-catalyzed cross-coupling reaction involving NDT-SnMe₃ and T-DPP-Br (Scheme 1). The large planar NDT unit was an attractive structural unit for constructing conjugated polymers, allowing for easy preparation of donor-acceptor architectures and showing potential for high-performance device. DPP is also a building block with highly planar features, consisting of a five-membered fused ring, further facilitating efficient stacking between polymer chains.^{11, 22, 28} T-DPP-Br, a monomer with a long aliphatic chain, was used to

overcome the low solubility of PNDT-type polymers, which seriously affects their processing properties.^{29,30} The alkylation process is highly productive and widely applicable, and we have reported the synthesis of a variety of similar DPP derivatives with various side chain lengths.³¹⁻³³ For efficient conjugated chain extension of the polymer, the polymerization process was carried out at high temperature for 72 hours. The resulting solid polymers were sufficiently soluble in the chlorobenzene solvent, appearing as a dark green solid powder, which was distinguished from the red color of dye T-DPP-Br in the monomeric state. After Soxhlet extraction, unreacted monomers, oligomers and undesired impurities present in the system were significantly removed.^{34,35} The purity of the material is further verified by the results of the elemental analyses in the Table S1, where it can be seen that the tested values for the content of the three elements were pretty close to the theoretical values. Figure S4 showed the infrared spectra of the polymer with the signature carbonyl peak appearing at 1664 cm⁻¹.



Scheme 1 (a) Synthesis of polymer PNDT-T-DPP.

The molecular weights of the dye polymer were determined by high-temperature GPC, and the results revealed extremely high molecular weights and well-dispersed properties (Đ). The average content of repeating units in each chain was calculated to be 48 and 136, respectively, based on the ratio of the number-average molecular weight (Mn) or the weight-average molecular weight (Mw) to the relative mass of the minimum repeating unit. The characterization data of the Z-mean molecular weight (Mz) and the molecular weight of the highest peak (Mp) of the polymer are shown in Figure S5. The high degree of polymerization indicates that the π -conjugation lengths of the PNDT-T-DPP are extremely long, which facilitates the narrowing of the energy level gap of the materials. On the other hand, the high molecular weight also contributed to the good thermal stability of the material. The thermal behavior of the polymer was further investigated by thermogravimetric analysis (TGA) and differential scanning calorimetry (DSC). On the basis of the TGA curve in Figure S6, it showed high thermal stability, with a 5% weight loss decomposition temperature (Td) of 400 °C and a mass retention of 20% at 600 °C. DSC results obtained according to Figure S7 indicated that there was no significant phase transition in the range of 30-250 °C.

Table 1. The molecular mass of PNDT-T-DPP obtained by high-temperature GPC.

| Mn | Mw | Đ ² | C ³ | H ³ | N ³ |
|----|----|----------------|----------------|----------------|----------------|
|----|----|----------------|----------------|----------------|----------------|

| | (Da) | (Da) | | (%) | (%) | (%) |
|-----------------------------|-------|--------|------|-------|------|------|
| PNDT-T-DPP | 54939 | 153087 | 2.79 | 75.09 | 8.99 | 2.59 |
| repeating unit ¹ | 1126 | 1126 | | 74.55 | 8.76 | 2.48 |

¹ The molecular chemical formula is C₇₀H₉₈N₂O₂S₄; ² $\bar{D} = Mw / Mn$; ³ Average of results from two separate tests.

Photophysics and electrochemical properties

Ultraviolet-visible (UV-vis) absorption spectroscopy was used to investigate the optical properties of the copolymer aggregates with long conjugated structures, in chloroform dilute solution and in the solid phase of thin films, respectively. The chloroform solution was chosen as the solvent because the polymers have good solubility in it. In both states, the polymers show broad absorption in the 300-1000 nm range with a triple absorption band and two shoulders (Figure 1a). Unlike most donor-acceptor structures, which tended to show distinct dual-absorption band features, the absorption characteristics here may be related to the NDT and the ratio of donor-to-acceptor occupancy.^{36,37} The absorption is relatively weak in the short wavelength ranges of 300 nm to 400 nm and 400 to 550 nm, with peaks at 305 nm and 420 nm, respectively. On the other hand, the absorption appears relatively high in the long wavelength range of 600 to 1000 nm, which is the result of intramolecular charge transfer.³⁸ The maximum absorption peak (λ_{onset}) is accompanied by a distinct shoulder, the 0-0 absorption peak. The significantly higher intensity of the 0-0 peak compared to the solution phase is related to the stronger stacking of the material in the thin film state. Meanwhile, the onset cut-off value (λ_{onset}) of absorption of the polymer in the thin film are redshifted by 70 nm compared to the absorption peaks in the solution phase, which are 996 nm and 925 nm, respectively, which is also related to the intermolecular π - π stacking in the thin film state. Calculations based on the result of λ_{onset} in the thin-film state indicate that the optical bandgap of the material is 1.24 eV.

To obtain the front-line orbital energy levels of the material, its HOMO and LUMO energy levels were tested by relying on the oxidation and reduction curves in cyclic voltammetry, respectively, and the corresponding plots are shown in Figure 1b. PNDT-T-DPP shows well reversible reduction features with its reduction onset peaks appearing at -0.78 V. We speculate that the reduction properties are related to the reversible reduction of the carbonyl group. Based on the position where the onset reduction peak appeared, it is presumed that its LUMO energy level is -3.62 eV with strong electron absorption ability. On the other hand, the oxidation curve of PNDT-T-DPP does not demonstrate reversible properties and its oxidation peak is not obvious. The positions of the reduction and oxidation peaks of the material appeared at -1.05 and +1.41 V, respectively. The HOMO energy level is estimated to be -5.60 eV based on the position of the onset of the oxidation peak at 1.20 V. The energy gap is calculated to be 1.98 V based on the difference between the HOMO energy level and the LUMO energy level, which is slightly different from that of the results obtained from the optical test. The difference in the energy level gap depending on electrochemical and photochemical measurements was evident due to the difference in the testing methods, which has been reported in other papers.³⁹ PNDT-T-DPP offers a high LUMO level and a proper HOMO level, which makes it potentially a hole-transporting P-type material compared

to electron-carrying ones. At the same time, the shallow HOMO level is favourable for charge injection and transport.⁴⁰

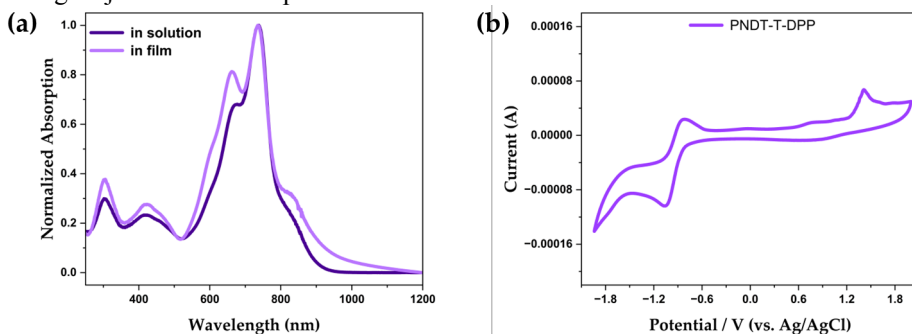


Figure 1 (a) UV-visible absorption characteristics of polymer PNDT-T-DPP in solution and in the annealed film state; (b) CV patterns of polymer PNDT-T-DPP film (positive swept of 500 mV/s).

Density functional theory (DFT) Calculation

We relied on theoretical simulations to investigate the optimal conformation of the material and its internal molecular arrangement. The long alkyl side chains were replaced by short methyl groups, while the polymer with long conjugation was further simplified to a dimer to minimize computationally costly time without compromising the accuracy of the calculations. For geometry optimization and frequency calculations, B3LYP functions and 6-31G (d, p) basis sets derived from Gaussian 16-based software were used to determine the optimal geometry of the dimer.⁴¹ DFT-D3 dispersion correction was adopted to further correct for weak interactions in order to enhance the accuracy of the calculations.⁴² Details of the spatial atomic coordinates of the dimer samples were provided in Table S2. The NDT motif consists of a fused ring of four aromatics showing excellent coplanarity and the distance between the sulfur atom (S) and the hydrogen atom (H) of the phenyl ring is 2.84 Å (Figure 2a). The T motif acts as a bridge group forming small dihedral angles within 1° with the NDT and DPP units, respectively, indicating that the single bonds here are not randomly distorted (Figure 2b). The distance between the hydrogen atom on the thiophene and the oxygen atom on the neighboring carbonyl group is only 2.10 Å, which is conducive to the formation of intramolecular hydrogen bonds. At the same time, the S atoms can form S...H with the DPP side chains. Figure 2c shows a side view of the dimer, further verifying the regularity and planarity of the molecular composition. The results of the analysis of the weak intramolecular interaction are shown in Figure 2d below, verifying the previous conjecture about the intramolecular mutual attraction (O...H, S...H, etc.).⁴³ Although the thiophene ring is attached to DPP through a single bond, O...H and S...H interaction forces can significantly limit ring-to-ring torsion (displayed in green or deep blue). Van der Waals forces and intramolecular attractions strongly contribute to the planarity of the material and further contribute to good layer-to-layer stacking. Figure 2e shows the distribution of electron-donating and electron-accepting groups within the molecule, with the carbonyl group showing a deep red color illustrating its strong electron-withdrawing properties.

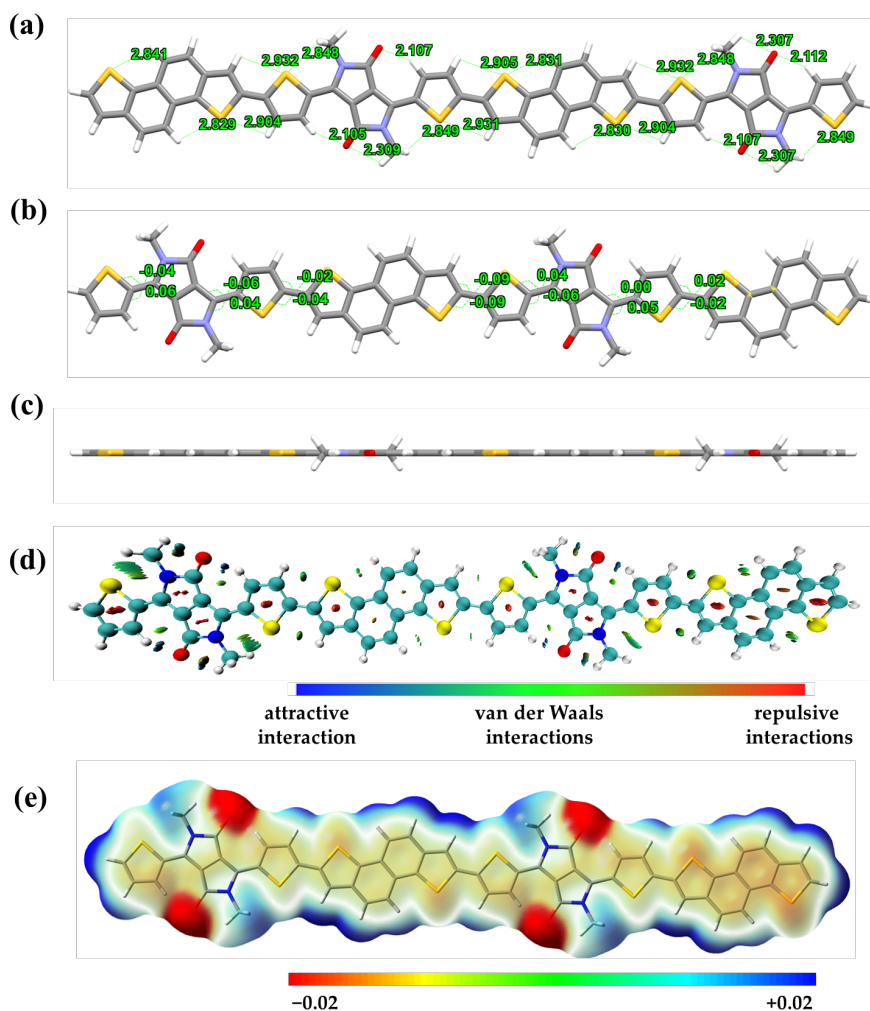


Figure 2 (a) Optimized conjugated backbone conformation; (b-c) Typical dihedral angle and; (d) Weak intramolecular interaction; (e) Electrostatic distribution of the methyl-substituted dimer of PNDT-T-DPP.

Figure 3 shows the molecular orbital diagram of the dimer. Both HOMO and LUMO on the conjugated segments of the donor and acceptor molecules are fully delocalized. Of these, LUMO is predominantly distributed on single bonds perpendicular to the long-axis direction, whereas HOMO dominates the double bonds along the long axis of the molecule. The calculated HOMO and LUMO energy levels are -5.20 eV and -3.30 eV, respectively, which are close to those obtained in the experiments via cyclic voltammetry. The HOMO-LUMO gap is therefore calculated to be 2.0 eV, which also matches the results of the CV-based tests. Orbital energy level analyses were performed using the Multiwfn software package. **Figure S8** shows the orbital diagram of LUMO+1/HOMO-1 accompanied by the orbital diagram of LUMO+2/ HOMO-2,

whose corresponding energy levels are $-3.12/-5.36$ eV and $-2.38/-6.04$ eV, respectively. The DFT simulated UV-Vis data (right side of Figure 3) support the actual UV test results, i.e. they all show a clear triple absorption band. Although the positions of their peaks are slightly varied, there is no significant difference in the positions of their absorption bands. The low-energy transition classified as ICT contributes the most in the visible region. The simulation results show that the maximum and onset absorption peaks of this dimer occur at 710 nm and 930 nm, respectively. The calculated optical gap (excitation energy of the first excited state) is only 1.33 eV, which is significantly different from that of the HOMO-LUMO gap due to the presence of the orbital coupling energy. There are obvious but reasonable variations between the frontier orbital energy levels derived from experimental and theoretical simulations. Considering the short effective conjugation length of dimers, there is a large discrepancy with the actual conjugation length of macromolecules.

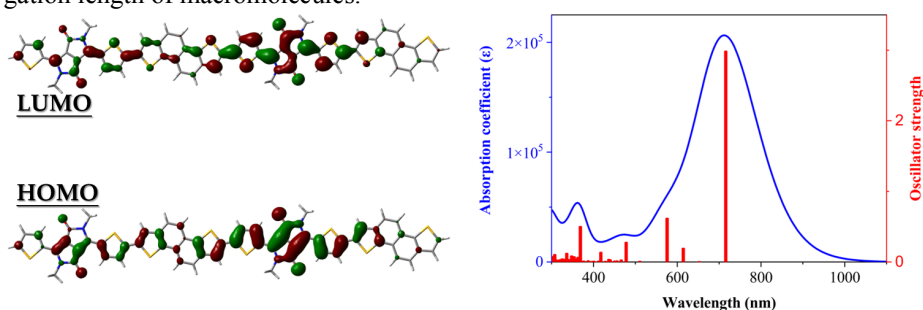


Figure 3 (left) Frontier orbital energy level diagram of the methyl-substituted dimer of PNDT-T-DPP; (right) DFT simulated UV-vis absorption curve.

PFET device performance

To characterize the electrical properties of this material in terms of charge carrier mobility, we fabricated PNDT-T-DPP based bottom gate top contact (BG/TC) structured PFET devices as shown in Figure S9a. The devices show a maximum hole mobility of $0.11 \text{ cm}^2 \text{ V}^{-1} \text{ s}^{-1}$ and reveal no electron mobility, which is typical of unipolar P-type materials (Figure S9b). As summarized in Table S3, the device achieves an average hole mobility of $0.09 \text{ cm}^2 \text{ V}^{-1} \text{ s}^{-1}$ and has the advantage of a small threshold voltage (V_{th}) and a high on-off current ratio (I_{on}/I_{off}). Moreover, by changing the device structure to bottom-gate-bottom-contact (BG/BC), the device mobility has been significantly improved. Table 2 summarizes the hole mobility extracted from the transfer characteristic curve (Figures 4a-d). Hole mobility was highest at an annealing temperature of $180 \text{ }^\circ\text{C}$. The maximum transport speed achieved was $0.35 \text{ cm}^2 \text{ V}^{-1} \text{ s}^{-1}$, and continuing to increase the temperature did not result in a significant improvement in the mobility. The modulation of temperature influenced the device performance of the materials under the same device preparation conditions. The output curves based on the PNDT-T-DPP device are shown in Figure 4e-f and Figure S8c.

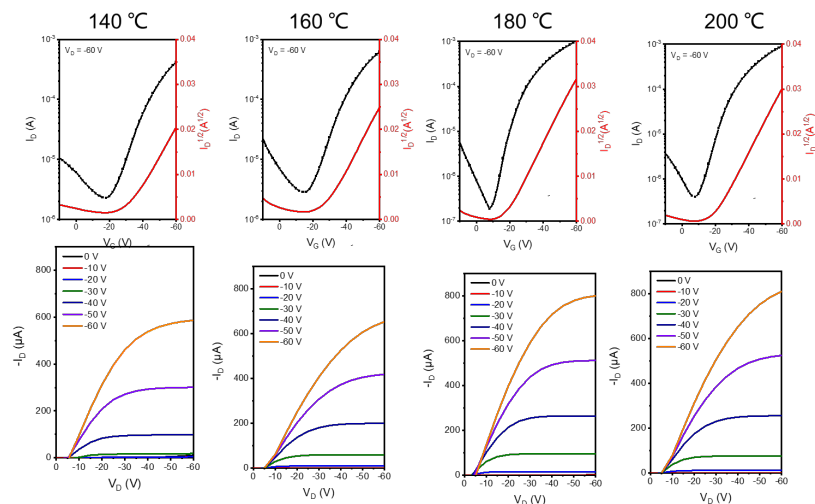


Figure 4 (a) Device configuration of BG/BC PFETs; Representative (b) transfer and (c) output characteristic curves based on PNDT-T-DPP device.

Table 2. Data summary of mobility of PNDT-T-DPP based BG/BC PFETs.

| Annealing Temperature (°C) | Mobility ($\text{cm}^2\text{V}^{-1}\text{s}^{-1}$) | V_{th} (V) | $I_{\text{on/off}}$ |
|----------------------------|--|---------------------|---------------------|
| 140 | 0.27 | -26 | 10^3 |
| 160 | 0.32 | -24 | 10^3 |
| 180 | 0.35 | -20 | 10^3 - 10^4 |
| 200 | 0.34 | -19 | 10^3 - 10^4 |

Photodiode device performance

The polymer PNDT-T-DPP also exhibits excellent light absorption properties in the near-infrared region (780-1000 nm), which further utilized to construct photodiode devices based on its unique narrow bandgap and wide absorption advantage, as shown in Figure 5a. The photodetector device structure was set as ITO (150 nm)/PNDT-T-DPP+PCBM (30 nm)/Al (100 nm). The current-voltage (I-V) curve indicates that the polymer PNDT-T-DPP exhibits more than an order of magnitude of photoresponsivity in the near infrared region (Figure 5b), which further indicates that PNDT-T-DPP-based polymers hold potential applications in organic optoelectronic devices such as photodiodes and photodetectors.

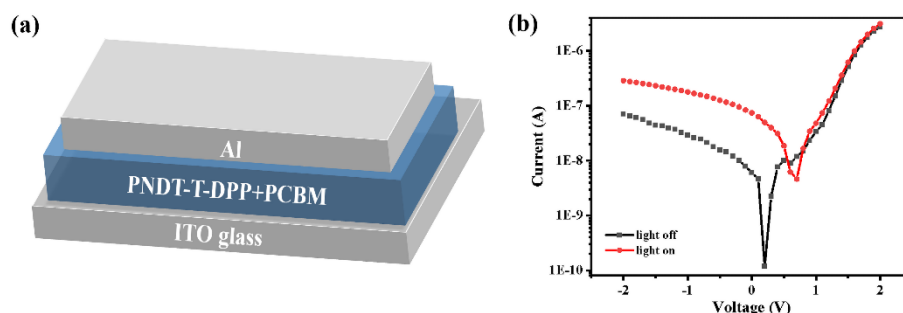


Figure 5 (a) Device structure of organic photodetector; (b) The I-V curve of the hybrid photoactive film under dark and 850 nm illumination at a light intensity of 1.26 mW cm^{-2} .

Microstructure and morphological analysis of PNDT-T-DPP film

Film morphology of the PNDT-T-DPP was investigated using atomic force microscopy (AFM). As shown in Figure 6a, the annealed films show fiber-like networks with a root-mean-square (R_q) roughness of 1.05 nm. The three-dimensional topography of the annealed film of PNDT-T-DPP was shown in Figure S10. The molecular stacking microstructure of PNDT-T-DPP in annealed films was also investigated by 2D-GIWAXS. The 2D diffraction pattern and corresponding 1D profile show in Figure 6b-d. The results indicate that the high-order ($h00$) diffraction peak along the out-of-plane (q_z) direction has appeared. The polymers show strong (100), (200), (300) and distinct (400) diffraction peaks, which indicate that they exhibit higher crystallinity.⁴⁴ The pronounced (010) diffraction peaks in-plane direction indicate that the material adopts a face-on stacking mode, which facilitates intermolecular charge hopping through strong π - π stacking. The π - π stacking and d-spacing distance of the polymer were calculated to be 3.69 Å and 20.26 Å, respectively, based on the Bragg equation (Table S4). In combination with AFM results, the polymer annealed films reveal good crystallinity without significant phase separation, which contribute to highly conductive hole migration. The face-on orientation favors a more compact and ordered long-range π - π stacking in the out-of-plane direction, which is beneficial for efficient charge transport in the photodiode and transistor devices, as discussed in the previous section.

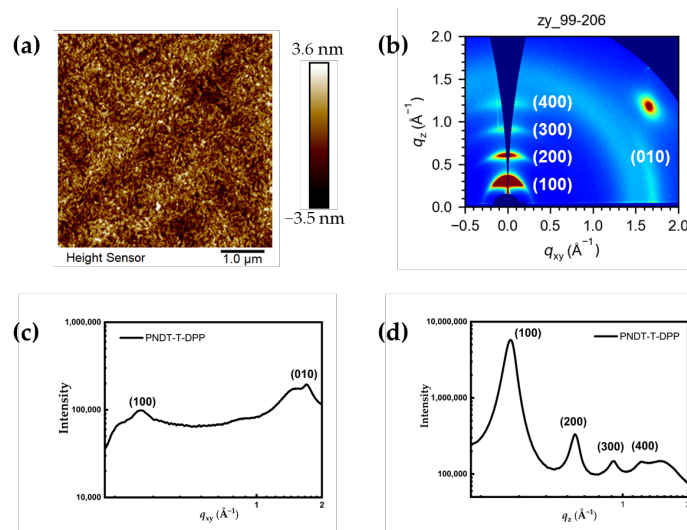


Figure 6 (a) AFM height image of annealed film; (b) 2D-GIWAXS pattern; (c-d) 1D-GIWAXS profile of polymer PNDT-T-DPP.

3 Conclusion

In summary, we prepared a high-yield synthetic route for the dye polymer PNDT-T-DPP by Stille cross-coupling polycondensation. Rational molecular design provides control of the molecular orbital energy distribution at the semiconductor frontier, allowing the derived polymer semiconductor to exhibit remarkable hole transport capability. The polymer itself has an extremely high molecular weight with an extended conjugation length, resulting in high thermodynamic stability and broad UV absorption properties. The materials synthesized based on molecular structure design strategies possess high coplanar regularity, which is further validated by DFT simulations. Moreover, the polymer shows excellent solvent processing and film-forming properties. The high crystallinity allows for a high hole transport efficiency of up to $0.35 \text{ cm}^2 \text{ V}^{-1} \text{ s}^{-1}$. The synthesis and application of related dye-based polymers as candidate materials for organic optoelectronic devices are still under laboratory research.

• Conflicts of interest

There are no conflicts to declare.

• Acknowledgements

This research was funded by China Post-doctoral Science Foundation (No. 2022TQ0399, No. 2024M753284), Gongbei Customs Scientific Research Fund Project (2023GK010), and the Shaoxing University grant (No. 13011001002/241). The authors thank the assistance from Shanghai Synchrotron Radiation Facility.

References

1. Q. Zhang, W. Hu, H. Sirringhaus and K. Müllen, *Adv Mater*, 2022, **34**, 2108701-2108704.
2. H. Sirringhaus, *Advanced Materials*, 2014, **26**, 1319-1335.
3. X. Chen, Z. Zhang, Z. Ding, J. Liu and L. Wang, *Angewandte Chemie International Edition*, 2016, **55**, 10376-10380.
4. F. Li, J. Zhou, J. Zhang and J. Zhao, *Materials*, 2024, **17**, 3362-3379.
5. L. Huang, F. Liu, J. Bao, X. Li and W. Wu, *Materials*, 2024, **17**, 1395-1410.
6. L. Luo and Z. Liu, *View*, 2022, **3**, 20200115-20200137.
7. M. Fahlman, S. Fabiano, V. Gueskine, D. Simon, M. Berggren and X. Crispin, *Nature Reviews Materials*, 2019, **4**, 627-650.
8. E. K. Lee, M. Y. Lee, C. H. Park, H. R. Lee and J. H. Oh, *Advanced Materials*, 2017, **29**, 1703638-1703667.
9. J. Chen, J. Kuang, Y. Liu, J. Yang, M. Zhu, X. Wei, M. Shao, Z. Zhao, Y. Guo, Y. Liu, *Advanced Optical Materials*, 2022, **10**, 2201243-2201251.
10. O. Ostroverkhova, *Chemical Reviews*, 2016, **116**, 13279-13412.
11. Q. Liu, S. E. Bottle and P. Sonar, *Advanced Materials*, 2019, **32**, 1903882-1903928.
12. Z.-F. Yao, J.-Y. Wang and J. Pei, *Chemical Science*, 2021, **12**, 1193-1205.
13. J. Yang, Z. Zhao, S. Wang, Y. Guo and Y. Liu, *Chem*, 2018, **4**, 2748-2785.
14. Y. Zhao, Y. Guo and Y. Liu, *Advanced Materials*, 2013, **25**, 5372-5391.
15. M. Sun, C. Zhang, S. Lu, S. Mahmood, J. Wang, C. Sun, J. Pang, L. Han and H. Liu, *Advanced Functional Materials*, 2024, DOI: 10.1002/adfm.202405471, 2405471-2405514.
16. Y. Zhou, W. Zhang and G. Yu, *Chemical Science*, 2021, **12**, 6844-6878.
17. Y. Wang and Y. Liu, *Trends in Chemistry*, 2023, **5**, 279-294.
18. X. Luo, H. Shen, K. Perera, D. T. Tran, B. W. Boudouris and J. Mei, *ACS Macro Letters*, 2021, **10**, 1061-1067.
19. M. Grzybowski and D. T. Gryko, *Advanced Optical Materials*, 2015, **3**, 280-320.
20. M. Kaur and D. H. Choi, *Chemical Society Reviews*, 2015, **44**, 58-77.
21. W. Zhuang, S. Wang, Q. Tao, W. Ma, M. Berggren, S. Fabiano, W. Zhu and E. Wang, *Macromolecules*, 2021, **54**, 970-980.
22. Y. Li, P. Sonar, L. Murphy and W. Hong, *Energy & Environmental Science*, 2013, **6**, 1684-1711.
23. S. A. L. Shaikh, S. S. Birajdar, S. D. Ambore, A. L. Puyad, P. Vijayanand, S. V. Bhosale and S. V. Bhosale, *Results in Chemistry*, 2022, **4**, 100473-100511.
24. W. T. Neo, W. T. Neo, Q. J. Ye, Z. Shi, S. J. Chua, S. J. Chua, J. Xu and J. Xu, *Materials Chemistry Frontiers*, 2018, **2**, 331-337.
25. I. Osaka, K. Komatsu, T. Koganezawa and K. Takimiya, *Science and Technology of Advanced Materials*, 2014, **15**.
26. I. Osaka, T. Abe, S. Shinamura and K. Takimiya, *Journal of the American Chemical Society*, 2011, **133**, 6852-6860.

27. P. J. Leenaers, A. J. L. A. Maufort, M. M. Wienk and R. A. J. Janssen, *The Journal of Physical Chemistry C*, 2020, **124**, 27403-27412.
28. Z. Yi, S. Wang and Y. Liu, *Advanced Materials*, 2015, **27**, 3589-3606.
29. I. Osaka, T. Kakara, N. Takemura, T. Koganezawa and K. Takimiya, *Journal of the American Chemical Society*, 2013, **135**, 8834-8837.
30. P. Dutta, H. Park, W.-H. Lee, K. Kim, I. N. Kang and S.-H. Lee, *Polymer Chemistry*, 2012, **3**, 601-605.
31. S. Ren, Z. Wang, W. Zhang, Y. Ding and Z. Yi, *Polymers*, 2023, **15**, 3713-3723.
32. S. Ren, Z. Wang, W. Zhang, A. Yassar, J. Chen and S. Wang, *Molecules*, 2024, **29**, 260-270.
33. S. Wang, L. Wang, S. Ren, W. Li, Z. Wang, Z. Yi and Y. Liu, *Advanced Electronic Materials*, 2024, DOI: 10.1002/aelm.202300816, 2300816-2300825.
34. J. Chen, Y. Jiang, J. Yang, Y. Sun, L. Shi, Y. Ran, Q. Zhang, Y. Yi, S. Wang, Y. Guo and Y. Liu, *ACS Applied Materials & Interfaces*, 2018, **10**, 25858-25865.
35. Z. Yi, Y. Jiang, L. Xu, C. Zhong, J. Yang, Q. Wang, J. Xiao, X. Liao, S. Wang, Y. Guo, W. Hu and Y. Liu, *Advanced Materials*, 2018, **30**, 1801951-1801958.
36. J. Chen, J. Yang, Y. Guo and Y. Liu, *Advanced Materials*, 2021, **34**, 2104325-2104355.
37. J. Yang, H. Wang, J. Chen, J. Huang, Y. Jiang, J. Zhang, L. Shi, Y. Sun, Z. Wei, G. Yu, Y. Guo, S. Wang and Y. Liu, *Advanced Materials*, 2017, **29**, 1606162-1606169.
38. J. Huang, Z. Mao, Z. Chen, D. Gao, C. Wei, W. Zhang and G. Yu, *Chemistry of Materials*, 2016, **28**, 2209-2218.
39. W. Jeong, K. Lee, J. Jang and I. H. Jung, *Polymers*, 2023, **15**, 1156-1170.
40. S. Zhang, W. Li, Y. Chen, Z. Wu, Z. Chen, Y. Zhao, Y. Wang and Y. Liu, *Chemical communications*, 2023, DOI: 10.1039/d3cc02510a, 9876-9879.
41. A. D. Becke, *Journal of Chemical Physics*, 1993, **98**, 5648-5652.
42. S. Grimme, A. Hansen, J. G. Brandenburg and C. Bannwarth, *Chem Rev*, 2016, **116**, 5105-5154.
43. T. Lu and F. Chen, *Journal of Computational Chemistry*, 2011, **33**, 580-592.
44. S. Ghosh, S. Shankar, D. S. Philips and A. Ajayaghosh, *Materials Today Chemistry*, 2020, **16**, 100242-100276.